Mengxue Zhang, Stephanie Ognier, Nadia Touati, Laurent Binet, Christophe Thomas, Patrick Tabeling and Michaël Tatoulian*

The development and numerical simulation of a plasma microreactor dedicated to chemical synthesis

DOI 10.1515/gps-2016-0086
Received May 1, 2016; accepted August 9, 2016; previously published online September 15, 2016

Abstract: A plasma microreactor dedicated to chemical synthesis has been conceived and developed using soft-lithography techniques. In this study, we propose to use highly reactive species created by the plasma discharge to replace traditionally used chemical initiators. A dielectric barrier discharge plasma was generated under atmospheric pressure and then dispersed into a continuous liquid phase with a T-junction geometry. Injected metal electrodes made it possible for in situ optical observations with an intensified charge-coupled device camera. No signal was detected when analyzing the exhaust liquid by electron spin resonance (ESR) spectroscopy. Numerical simulations confirmed that only low quantities of hydroxyl radicals could diffuse into the liquid phase, giving a concentration of DMPO-OH of 10^{-6} mol/l, below the detection limit of ESR.

Keywords: ESR; hydroxyl radical; iCCD; microreactor; plasma.

***Corresponding author: Michaël Tatoulian,** PSL Research University, Chimie Paristech-CNRS, Institut de Recherche de Chimie Paris, 75005 Paris, France, e-mail: michael-tatoulian@chimie-paristech.fr
Mengxue Zhang, Laurent Binet and Christophe Thomas: PSL Research University, Chimie Paristech-CNRS, Institut de Recherche de Chimie Paris, 75005 Paris, France
Stephanie Ognier: PSL Research University, Chimie Paristech-CNRS, Institut de Recherche de Chimie Paris, 75005 Paris, France; and UPMC-Univ Paris 06, 75005 Paris, France
Nadia Touati: PSL Research University, Chimie Paristech-CNRS, Institut de Recherche de Chimie Paris, 75005 Paris, France; and University Nord de France, Lille1, LASIR (UMR CNRS A8516), 59655, Villeneuve d'Ascq Cedex, France
Patrick Tabeling: Laboratoire Microfluidique, MEMs et Nanostructures, ESPCI ParisTech, UMR Gulliver 7083, ESPCI, CNRS, 10 Rue Vauquelin, 75005 Paris, France

1 Introduction

Living polymerizations, introduced in 1956 by Szwarc [1], proceed in the absence of chain termination and chain transfer steps, while maintaining instantaneous initiation and uniform growth of each propagating species. Controlled living radical polymerizations, once thought unobtainable [2], have now been realized through many versatile processes such as catalytic chain-transfer polymerization, atom-transfer radical polymerization, and reversible addition-fragmentation chain-transfer polymerization. Such processes allow macromolecules to be prepared with precisely controlled molecular weights (Mn) and narrow molecular weight distributions (Mw/Mn). Nevertheless, these methods may involve transition state metal as catalysts, which somehow raises the separation problem at the end of the reaction [3].

Recently, the organic synthesis by plasma technology is drawing more and more attention from chemists. The plasma generates a large amount of reactive species (electrons, metastables, positive and negative ions, etc.) and therefore promotes various chemical reactions [1]. Engaging fewer reactions and catalysts and consuming less solvent, plasma-assisted reactions open up new and cleaner routes for organic synthesis.

Osada et al. [4] and Li et al. [5] have presented a novel approach to prepare polymers with the aid of a plasma. The initiation takes place in the gas phase with radicals produced by the plasma, whereas propagation and termination steps are continued in the liquid. The molecular weight of polymer is greatly increased in plasma-initiated reactions. Nevertheless, the plasma technology sometimes shows the disadvantage of low selectivity due to the highly reactive nature of radicals [6]. Microfluidics, known for its precise handling of fluid hydrodynamics [7], turns out to be an ideal tool to control the radical diffusion at the interface between the plasma and the liquid.

In this study, a plasma integrated microfluidics device has been developed for chemical synthesis. The transfer of reactive species (especially radicals) from the gas phase

to the liquid phase is tuned by the multiphase flow. A high transfer efficiency is ensured by the high surface/volume ratio of plasma bubbles. Yamanishi et al. [8] presented a microreactor which generates mono-dispersed microscale plasma bubbles under atmospheric pressure. Discoloring of indigo carmine solution by plasma bubbles is shown in this study to demonstrate the diffusion of hydroxyl radicals, whereas the decomposition of the dye molecule may as well be a result of hydrogen peroxide production by plasma. The migration of hydroxyl radicals from gas to liquid phase is evaluated by electron paramagnetic resonance spectroscopy. Our plasma-integrated gas-liquid microreactor developed in this study inspires a new route for chemical synthesis.

2 Materials and methods

2.1 Microfabrication processes

The plasma microreactors were made by soft imprint lithography based on methods described in the works of Bartolo et al. [9] and Priest [10] with the thiolene-based resin Norland Optical Adhesive 81 (NOA 81, Norland Products Inc., Cranbury, NJ, USA). This optical glue was chosen over traditionally used polydimethylsiloxane (PDMS) for its good physical, chemical, electrical, and optical properties: (1) unlike PDMS devices, NOA 81 microreactors are impermeable to gas such as air and water vapor, which ensures a enclosed environment for plasma [9]; (2) cured NOA 81 has a high elastic modulus (typically 1 GPa), which avoids sagging effects [9]; (3) NOA 81 appears less sensitive to solvent swelling effects than PDMS [9]; (4) the dielectric constant of NOA 81 being 4.05 at 1 MHz, it is as well a performant insulating material; (5) with a high transmittance in the visible and near-UV range, NOA 81 makes it possible for in situ discharge diagnostics (optical emission spectroscopy or ultra-rapid camera measurements). Owing to these properties, NOA 81 is a good candidate for the fabrication of plasma microreactors.

Another important factor for plasma microreactors is the electrodes fabrication. Here in our study, we used electrodes using microsolidics technique [11]. Figure 1 shows the main steps for the fabrication of a plasma microreactor with solidified electrodes. First, using photolithography, we obtained a micropatterned SU-8 thin layer on a Si wafer. The first replica of these micropatterns was realized by PDMS (RTV-615, MG Chemicals, Surrey, British Columbia, Canada) molding (Figure 1A). These PDMS molds were later used to make NOA 81 stickers with microstructured patterns. Two main techniques were employed for the fabrication of NOA stickers, either by stamp technique or by capillarity technique (Figure 1B) [9]. For the stamp technique, several drops of NOA 81 liquid were firstly deposited on a rigid substrate (glass slide, cover slide, Si wafer, etc.). Then the PDMS mold was placed on the NOA 81 liquid, followed by a short UV illumination to partially insulate the NOA 81 while keeping a thin layer of uncured polymer on the surface. As for the second technique, the PDMS mold was firstly put in contact with the rigid substrate, while the NOA 81 liquid was deposited around the PDMS mold afterwards. The polymer liquid would fill in the microstructures of PDMS mold, driven by capillary forces. A short UV illumination was also used for the partial insulation of NOA stickers. Three assembly methods were envisaged for the microfluidic device fabrication. NOA stickers made by either stamp technique or capillary technique may be sealed with another pre-drilled rigid substrate (Figure 1C (II)(III)), whereas these NOA stickers may be also sealed with another pre-drilled NOA sticker (Figure 1C (I)). Once the microfluidic device was closed, it was put on a hot plate for the injection of metallic electrodes (Figure 1D). The material used for the electrodes was an alloy with 52% In and 48% Sn (Indium Corporation of America, Utica, NY, USA).

2.2 T-junction geometry for gas/liquid emulsion

As for the geometry of the plasma microreactor, a T-junction design was used for the generation of bubbles. Garstecki et al. [12] have employed this geometry to controllably generate monodispersed bubbles with and without surfactants at low-to-moderate Reynolds numbers (Re between 0.01 and 10). Figure 2A shows the design of a plasma microreactor with T-junction. With this fabrication process, electrodes were located on the sides of the gas inlet channel, which ensured the possibility of optical observation of plasma discharges. Figure 2B shows a microfluidic plasma reactor with solidified electrodes. For the studied plasma microreactor, $d_g = 120$ μm, $d_l = 240$ μm. The height of the microchannels was $h = 50$ μm. The main channel length (from the T-junction to the outlet) was 2 cm. The liquid phase was 2-propyl alcohol (IPA, RECTAPUR, VWR International S.A.S, Fontenay-sous-Bois, France) or deionized water (Milli-Q water purification system, Merck Millipore, Molsheim, Alsace, France), while the working gas was argon (Alphagaz 1 Argon, Air Liquide, Paris, France). The pressure controller (Fluigent, MCFS-EZ system, Paris, France), regulated by the computer, gave rise to a stable bubble generation within the flow-focusing geometry. The flow rate of the liquid phase varies between 0 and 100 μl/min for IPA flow and between 0 and 50 μl/min for deionized water. The flow rates of the gas phase are estimated by post-treatments of bubble images and vary from 10^{-2} to several sccm. Figure 3 shows the segmented gas-liquid flow generated by the T-junction. Argon gas was dispersed into the main channel with the liquid phase as the continuous phase. As shown in Figure 3A and B, the gas/liquid flow was more stable with IPA than with deionized water, indicated by more regular bubble forms and more stable bubble generation frequencies for the IPA flow. This difference in flow behaviors may result from the difference in surface tension: IPA has a lower surface tension than water. No surfactant was added in water deliberately since surfactant molecules may interfere with the radical diffusion at the gas/liquid interface. As presented in the work of Garstecki et al. [12], it is somehow difficult to control bubble sizes when the discretized phase adheres to the channel wall (the case for water free of surfactant with NOA channel walls).

2.3 The plasma generation and observation

The two electrodes of the microreactor are connected, respectively to a high-voltage source and the ground. Sinusoidal waves generated by a function generator are magnified by a signal amplifier (Trek 20/20C, Trek Inc., Lockport, NY, USA) to several tens of thousands of volts. Figure 4 illustrates the experimental set-up for the observation of plasma discharges. A current probe (Pearson Current Monitor, model

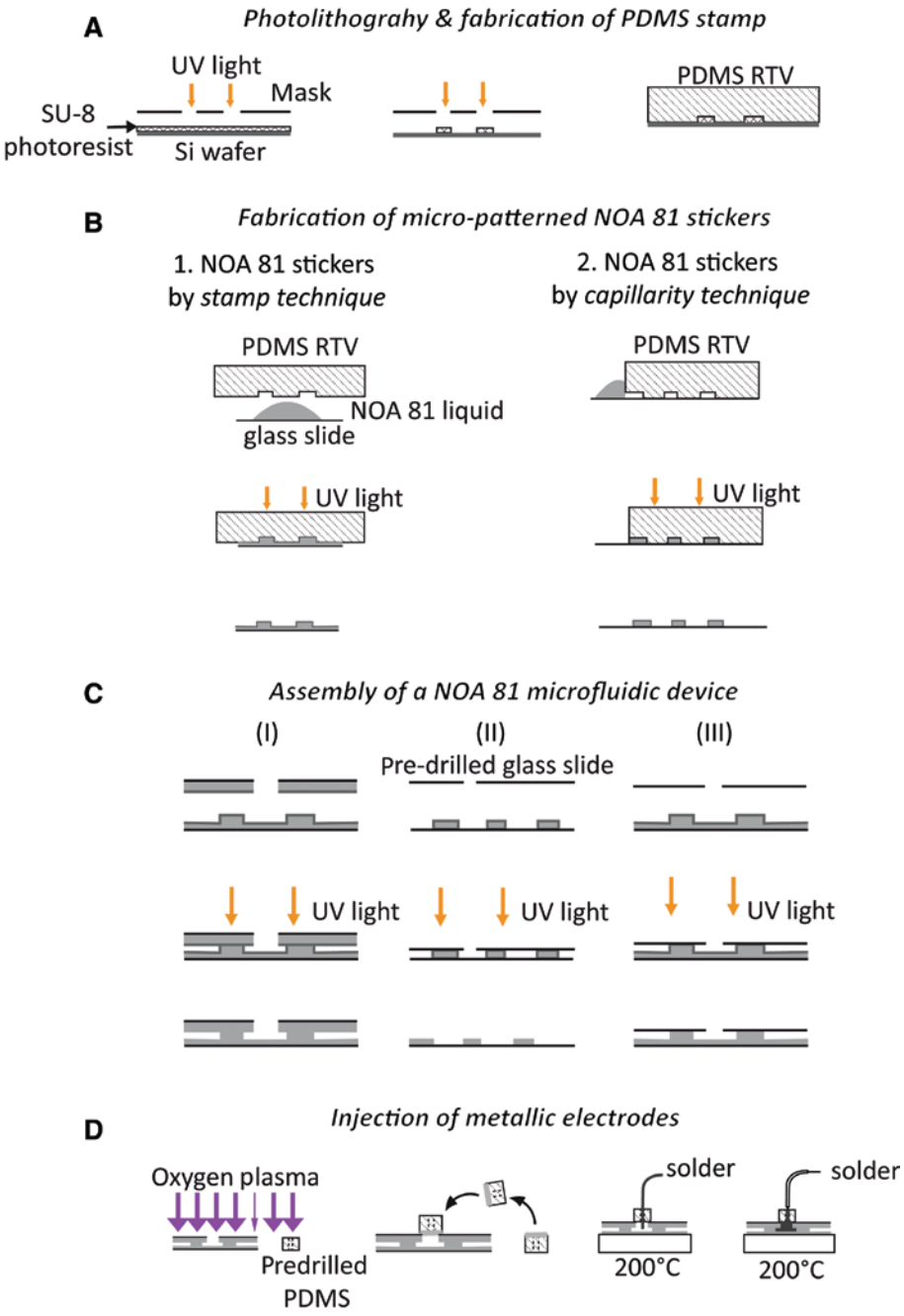

Figure 1: Fabrication steps of a plasma microreactor with solidified electrodes. (A) Photolithography and fabrication of PDMS stamp; (B) fabrication of micro-patterned NOA 81 stickers; (C) assembly of a NOA 81 microfluidic device; (D) injection of metallic electrodes.

2877, 200 MHz, Pearson Electronics, Palo Alto, CA, USA) is placed between the microreactor and the ground connection, in order to electrically detect plasma discharges. In this experiment, plasma discharges were observed when the high-voltage source achieved 9 kV as peak-to-peak value at 500 Hz. An intensified charge-coupled device (iCCD) camera (Pimax4, Princeton Instruments, Trenton, NJ, USA) is used to collect images of plasma discharges through a macroscope (Leica Z16 APO, Leica Microsystemes SAS, Nanterre, France). A dark environment is indispensable for the detection of weak optical emission of electrical discharges.

2.4 Electron spin resonance spectroscopy measurements

Since radicals are important initiators for chemical synthesis, the diffusion of radicals (hydroxyl radicals in this study) generated by plasma into the liquid phase was studied by the electron spin resonance (ESR) spectroscopy.

Wu et al. [13] demonstrated the generation and diffusion of hydroxyl radicals (·OH), superoxide anion radicals ($\cdot O_2^-$), and

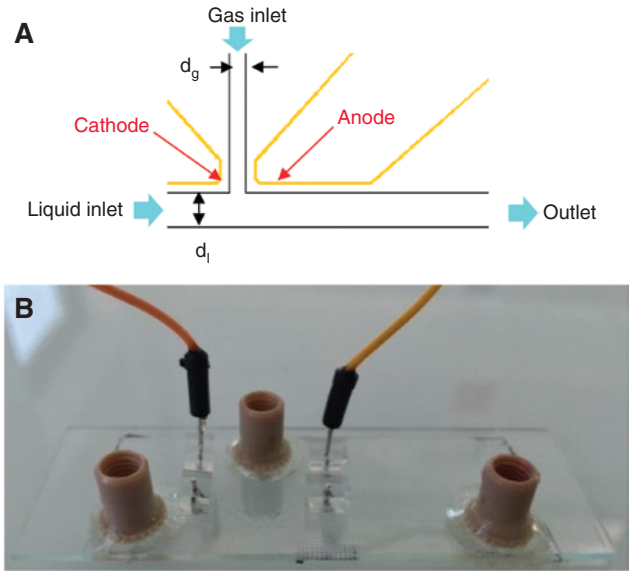

Figure 2: Schematic drawing (A) and image (B) of a T-junction plasma microreactor.

singlet oxygen ($^1O_2$) in a gas/liquid plasma reactor with ESR spectroscopy. The use of spin trapping agents such as 5,5-dimethyl-1-pyrroline N-oxide (DMPO, Interchim, Montluçon, France) avoids the diagnosis problem due to the short life span of radical species (Figure 5A).

2.5 Numerical simulation of OH radical trapping in the plasma microreactor

A simplified 1-D model (COMSOL Multiphysics, COMSOL France, Grenoble, France) was established to estimate the quantity of spin-adduct in the liquid phase with various experimental parameters (the initial concentration of DMPO, the bubble size, and the gas/liquid ratio). The studied zone is represented as a red and blue line in Figure 5B, with the red segment representing the gas phase and the blue segment representing the liquid phase. We supposed that the species distribution is symmetric in the gas bubble as well as in the liquid slug. Therefore, we only studied the diffusion and reaction in half a bubble and half a liquid slug.

In the present model, mass transfer is supposed to occur purely by diffusion in both phases using 10^{-5} and 10^{-9} m^2 s^{-1} as diffusion coefficients in gas and liquid phases, respectively. The basic species transport equations solved in the liquid and gas were therefore as follows:

$$\frac{\partial c_i}{\partial t} + \nabla(-D_l \nabla c_i) = R_i \quad (1)$$

$$\frac{\partial c_i}{\partial t} + \nabla(-D_g \nabla c_i) = R_i \quad (2)$$

Where c is the concentration of chemical species i (mol/m^3), t is the time (s), and D_g and D_l are the diffusion coefficients (m^2/s) in the gaseous phase and in the liquid phase, respectively. In these equations, chemical reactions are modelled as source terms R_i.

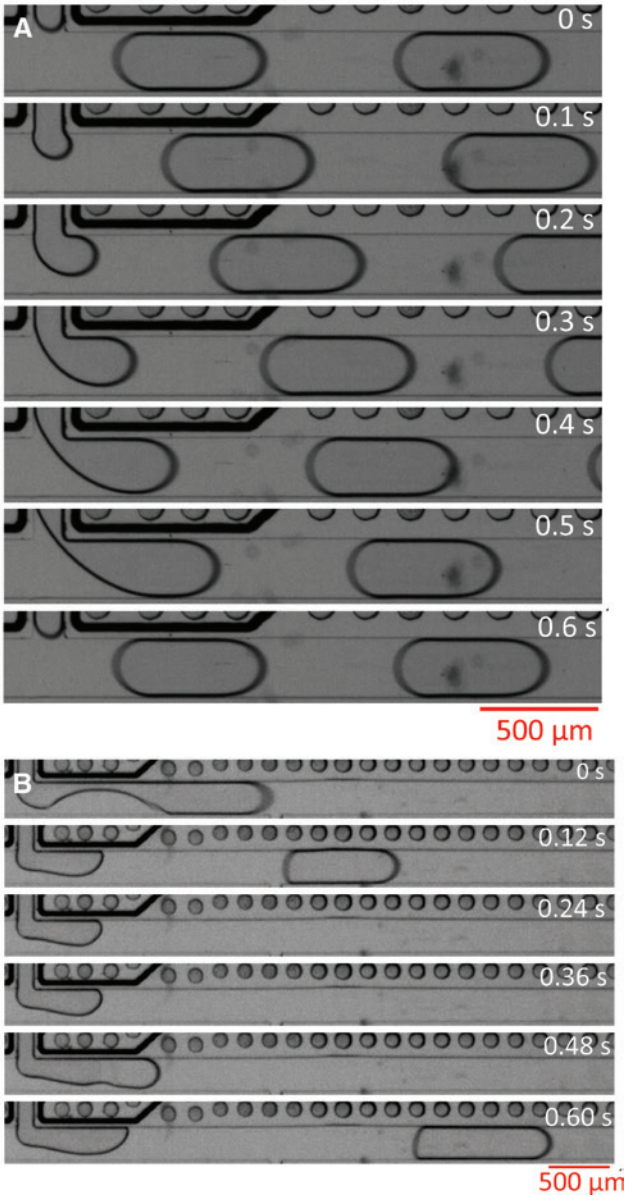

Figure 3: Flow dynamics of the gas/liquid segmented flow: the gas phase is argon; the liquid phase is 2-propyl alcohol (A) and deionized water (B).

Reactions in the gas phase and in the liquid phase (Figure 5C) are described in Tables 1 and 2.

Based on the spin-trapping reaction (Reaction 12 in Table 2), the molar reaction rate of DMPO-OH creation is given by

$$R_{\mathrm{DMPO-OH}} = k_{12} \cdot [\mathrm{DMPO}]_l \cdot [\mathrm{OH}]_l \quad (3)$$

Where k_{12} is the reaction rate constant of Reaction 12 (Table 2), $[\mathrm{DMPO}]_l$ is the concentration of DMPO in the liquid phase, and $[\mathrm{OH}]_l$ represents the hydroxyl radical concentration in the liquid phase.

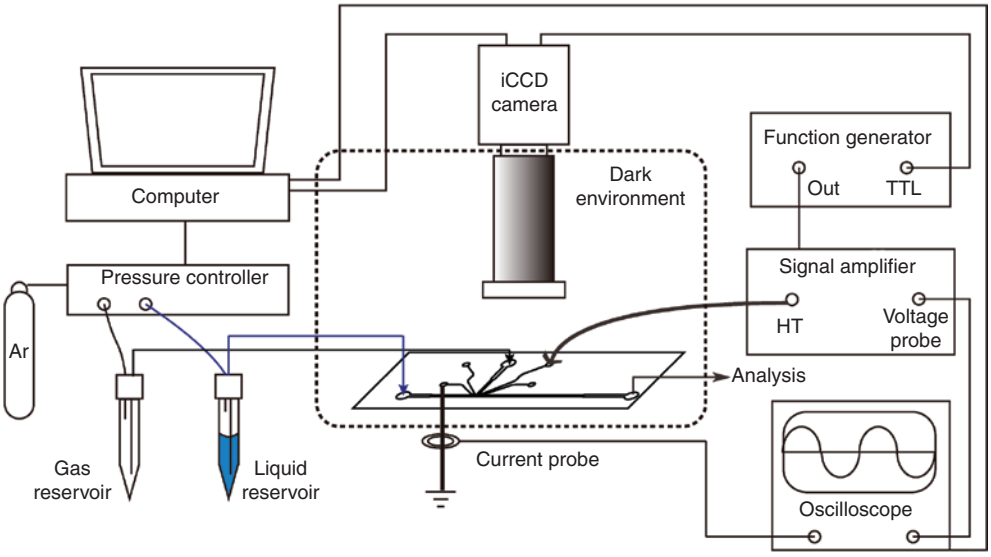

Figure 4: Schematic illustration of the experimental setup for optical measurement of the plasma microreactor.

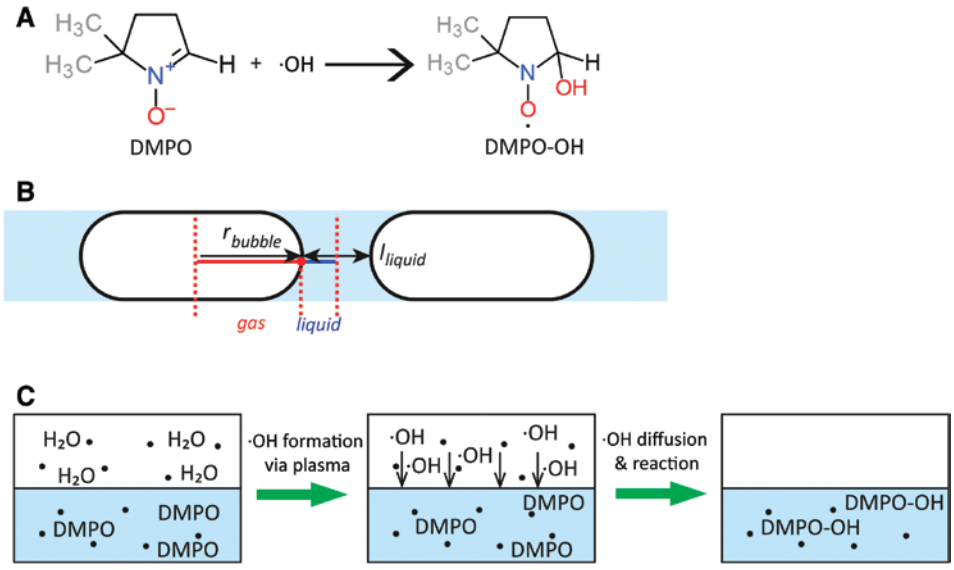

Figure 5: Spin trapping reaction between DMPO and hydroxyl radicals. (A) The chemical equation of the spin trapping reaction; (B) the geometry configuration of the gas/liquid flow; (C) schematic illustation of the spin-trapping process.

We assumed that each bubble, when squeezed into the main channel, carried 36 ppm of hydroxyl radicals in the gas phase [17]. This concentration was hypothesized assuming that argon is saturated in water vapor and in accordance with the works of Hibert et al. [17] and Bruggeman and Schram [18]. The size of gas slugs and liquid slugs are represented by r_{bubble} and l_{liquid}.(Figure 5B). In the present model, mass transfer is supposed to occur purely by diffusion in both phases using 10^{-5} and 10^{-9} m^2 s^{-1} as diffusion coefficients in gas and liquid phases, respectively. It is also assumed that there is a thermodynamic equilibrium between interfacial phase concentrations for ·OH and H_2O_2 species. The Henry constant of hydroxyl radicals in the gas phase is 760 mol m^{-1} Pa^{-1} [19].

3 Results and discussion

3.1 Plasma diagnosis

Due to the small size of the microreactor and the weak intensity of plasma discharges, it was extremely complicated to observe plasma discharges by eye directly. Two aspects of plasma discharges are presented here. Figure 6A shows the electrical measurement of plasma discharges. A

Table 1: Dominant reactions in the gas phase.

No	Reaction	*k*
1	$H\cdot + \cdot OH \rightarrow H_2O$	4.14×10^{6} m^6/(mol^2 s) [14]
2	$\cdot OH + \cdot OH \rightarrow H_2O_2$	1.05×10^{7} m^6/(mol^2 s) [14]
3	$\cdot OH + \cdot OH \rightarrow H_2O + O\cdot$	8.9×10^{5} m^3/(mol s) [14]
4	$\cdot OH + H_2 \rightarrow H_2O + H\cdot$	4.033×10^{3} m^3/(mol s) [14]
5	$\cdot OH + H_2O_2 \rightarrow H_2O + HO_2$	1.02×10^{6} m^3/(mol s) [14]
6	$H\cdot + \cdot H \rightarrow H_2$	9.7×10^{4} m^6/(mol^2 s) [15]
7	$H_2O_2 + H\cdot \rightarrow \cdot OH + H_2O$	2.52×10^{4} m^3/(mol s) [15]
8	$H_2O_2 + H\cdot \rightarrow H_2 + HO_2$	3.1×10^{3} m^3/(mol s) [15]
9	$O\cdot + HO_2 \rightarrow \cdot OH + O_2$	3.5×10^{7} m^3/(mol s) [14]
10	$\cdot OH + HO_2 \rightarrow H_2O + O_2$	6.62×10^{7} m^3/(mol s) [14]
11	$HO_2 + HO_2 \rightarrow H_2O_2 + O_2$	9.63×10^{5} m^3/(mol s) [14]

Table 2: Dominant reactions in the liquid phase.

No	Reaction	*k*
12	$DMPO + \cdot OH \rightarrow DMPO\text{-}OH$	10^{6} m^6/(mol^2 s) [16]
13	$\cdot OH + \cdot OH \rightarrow H_2O + O\cdot$	1.05×10^{7} m^3/(mol s) [14]
14	$\cdot OH + O\cdot \rightarrow O_2 + H\cdot$	8.9×10^{5} m^3/(mol s) [14]
15	$\cdot OH + H\cdot \rightarrow H_2O$	4.033×10^{3} m^6/(mol^2 s) [14]
16	$\cdot OH + HO_2 \rightarrow H_2O + O_2$	1.02×10^{6} m^3/(mol s) [14]
17	$\cdot OH + H_2 \rightarrow H_2O + H\cdot$	9.7×10^{4} m^3/(mol s) [14]
18	$H_2O_2 + \cdot OH \rightarrow HO_2 + H_2O$	2.52×10^{4} m^3/(mol s) [14]
19	$\cdot OH + \cdot OH \rightarrow H_2O_2$	3.1×10^{3} m^6/(mol^2 s) [14]
20	$O\cdot + HO_2 \rightarrow \cdot OH + O_2$	3.5×10^{7} m^3/(mol s) [14]
21	$\cdot OH + HO_2 \rightarrow H_2O + O_2$	6.62×10^{7} m^3/(mol s) [14]
22	$HO_2 + HO_2 \rightarrow H_2O_2 + O_2$	9.63×10^{5} m^3/(mol s) [14]

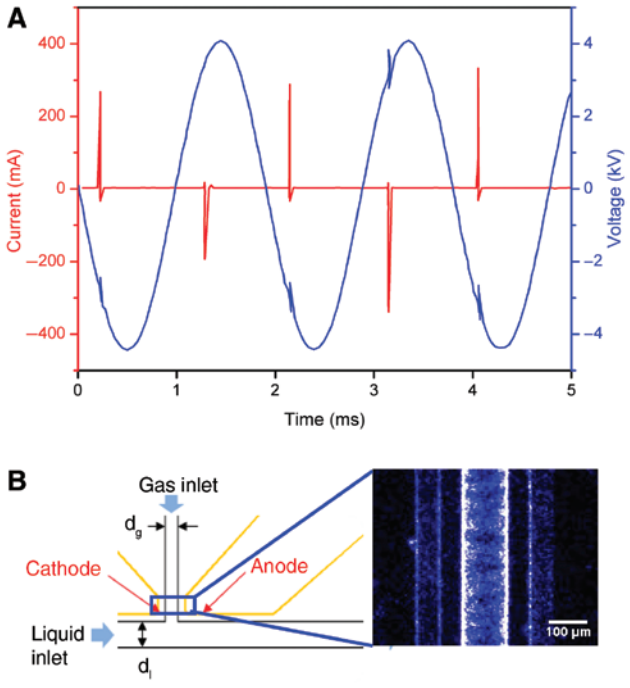

Figure 6: Electrical diagnosis (A) and optical diagnosis (B) of the plasma.

discharge was generated every half period as indicated by the current peak visible in Figure 6A.

Figure 6B shows the electrical discharges in the vicinity of the T-junction using iCCD camera. The internal trigger mode was used with a gate delay of 25 ns and a gate width of 2 ms. We observed an emission of photons of the gas phase between the two electrodes, which proved the ignition of the plasma. We can as well figure out the outlines of the two electrodes in the iCCD image because of their reflecting surfaces.

3.2 Study of spin trapping reaction

An aqueous solution of DMPO was prepared with a concentration of 0.05 mol/l for the spin trapping reaction. The pressures for the gas and the liquid inlet were both 90 mbar. After the T-junction, the gas/liquid segmented flow continued travelling several minutes before reaching a reservoir for ESR spectroscopy. It is to be noted that the production of hydroxyl radicals in the gas phase should only happen before the formation of gas slugs since no discharges were possible at the downstream of the T-junction. The gas slug length was $2r_{bubble} = 870$ µm, and the liquid slug length was $l_{liquid} = 1900$ µm. However, no DMPO-OH signal was detected by the ESR spectroscopy.

We used mathematical tools to estimate the concentration of DMPO-OH at the outlet of the microreactor. For the experimental condition ($r_{bubble} \approx 500$ µm, $l_{liquid} \approx 2000$ µm), the final concentration of DMPO-OH calculated by the model was inferior to 10^{-8} mol/l. Because the sensitivity of our ESR spectroscopy apparatus goes down to ~10^{-6} mol/l, there was no way that a spin adduct signal could be detected experimentally.

Using the numerical simulation, a parametric study was carried out to study the influence of the initial concentration of DMPO ($[DMPO]_0$), the bubble size (r_{bubble}), and the liquid/gas ratio (l_{liquid}/r_{bubble}) on the final concentration of DMPO-OH. The objective was to determine the highest possible spin-adduct concentration under optimum operating conditions. Prior studies on the fluid dynamics of the gas/liquid flow showed that it was complicated to generate tiny liquid slugs with large gas slugs; therefore, the liquid/gas ratio range was chosen between 0.5 and 40. Figure 7A shows that the final concentration of DMPO-OH increases as the initial DMPO concentration increases, whereas the final [DMPO-OH] reaches a plateau level when the initial concentration of DMPO gets to around $10^{-3} \sim 10^{-2}$ mol/l. In the liquid, the reaction of OH radicals with DMPO competes with the recombination of OH radicals into H_2O_2. The higher the concentration of DMPO, the more selective the

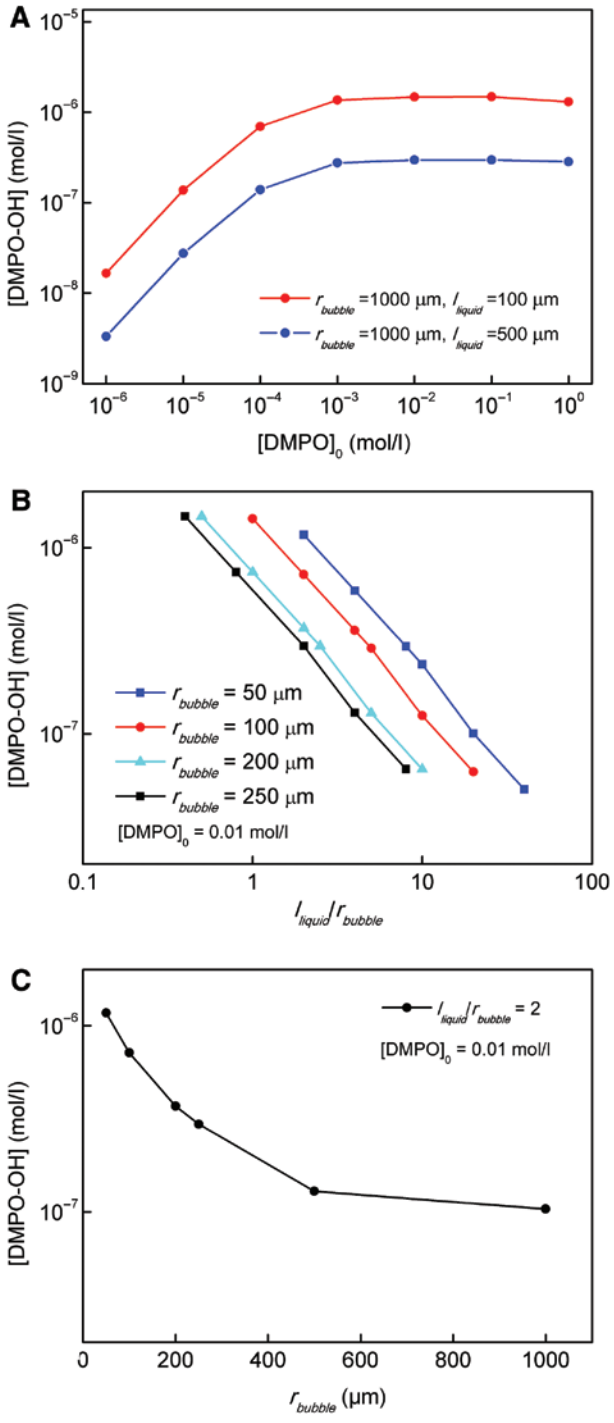

Figure 7: Model predictions of the final spin adduct concentration: (A) at different initial DMPO concentrations; (B) at different lliquid/r_{bubble} ratios; (C) at different bubble sizes.

reaction between OH radicals and DPMO, explaining the increase of DMPO-OH in the first part of the curve. When the DMPO concentration exceeds 10^{-3} mol/l, the selectivity is around 100%, and a plateau is reached. This plateau level is determined by the size of the plasma bubble and the liquid thickness. Figure 7B shows that the final concentration of DMPO-OH decreases as the l_{liquid}/r_{bubble} ratio gets higher, while $[DMPO]_0$ remains 0.01 mol/l and the gas slug size remains the same. Since the spin trapping reaction happened at the gas/liquid interface afterall, the more segmented the liquid phase was, the more OH radicals could be trapped into the liquid phase. For the gas bubble size, Figure 7C indicates that the final concentration of spin adduct decreases as the bubble size increases, while the initial DMPO concentration and the l_{liquid}/r_{bubble} ratio stay unchanged. This result can be explained as follows: the larger the bubble size, the higher the fraction of gaseous OH radicals which recombined in gaseous H_2O_2 before reaching the gas-liquid interface. Finally, the simulation work indicated an upper limit for the final concentration of spin-adduct in the liquid phase of around 10^{-6} mol/l, which corresponds to the sensitivity threshold of the ESR analysis. According to the simulation, ESR analysis is therefore not sensitive enough to be used with the plasma microreactor used in this study.

3.3 Outlook: Plasma ignition in moving bubbles

The low level of spin-adduct concentration was directly related to the low concentration of hydroxyl radicals generated in the gas bubble. The measurement of Hibert et al. [17] by resonant absorption spectroscopy indicates that the OH radical production in an argon-water mixture is around 36 ppm. The quantity of hydroxyl radicals delivered by each gas bubble to the liquid phase was quite limited, which led to a low spin-adduct concentration. In order to have more hydroxyl radicals diffused into the liquid phase, a solution is to ignite the plasma discharge several times during the passage of the bubble along the main channel, so that a higher amount of radicals can be generated and then transferred into the liquid.

To realize this, a similar microdevice with electrodes injected on each side along the main channel was fabricated (Figure 8). The main channel dimensions of this device are the following: $w_g = w_{out} = 240$ µm; $w_o = w_d = 1/2w_g = 120$ µm; $h = 80$ µm. With this device, it was possible to ignite several times the plasma discharge during the passage of the bubble in the channel using the following conditions: $p(Ar) = 86$ mbar, $p(H_2O) = 88$ mbar, high voltage = 12.51 kV, frequency = 200 Hz. An illuminated plasma bubble has been observed travelling through the main channel, which shows a continuous ignition of plasma in the reactor (Figure 9). More experiments are underway to quantify how many OH radicals

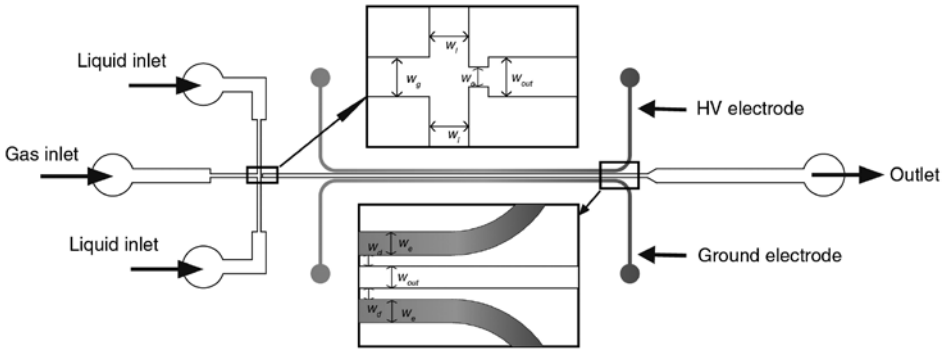

Figure 8: A plasma microreactor in which the plasma can be regenerated in gas bubbles along the main channel.

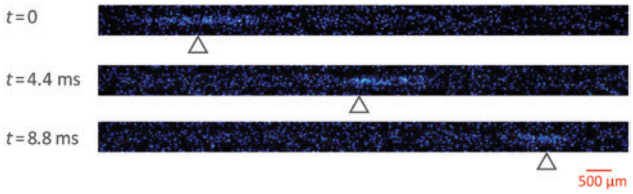

Figure 9: Optical diagnosis for continuous ignition of a plasma bubble in the main channel (internal trigger, gate width 500 µs, gate delay 400 µs, 10 accumulations).

can be injected in the liquid phase using this new microdevice. A European patent has been applied with the latter design [20].

4 Conclusions

For the present study, a plasma microreactor dedicated to chemical synthesis has been developed using lithography techniques. The production of mono-dispersed plasma microbubbles in a T-junction microreactor was demonstrated. The production and diffusion of hydroxyl radicals into the liquid phase was evaluated by numerical simulation. The method of ESR spectroscopy was developed for the identification of hydroxyl radicals in the liquid phase.

The present microreactor has been proven to present a low concentration of OH radicals in the liquid phase, which can be a good configuration for using plasma-generated radicals as polymerization initiators. However, for more radical-demanding chemical reactions, an ignition of plasma along the main channel will be necessary to inject higher amounts of hydroxyl radicals in the liquid phase.

Acknowledgments: This work has received the support of Institut Pierre-Gilles de Gennes (laboratoire d'excellence, "Investissements d'avenir" program ANR-10-IDEX-0001-02 PSL and ANR-10-LABX-31, équipement d'excellence, "Investissements d'avenir" program ANR-10-EQPX-34).

References

[1] Szwarc M. *Nature* 1956, 178, 1168–1169.
[2] Yamada B, Zetterlund PB. In *Handbook of Radical Polymerization*, Davis, TP, Ed., John Wiley and Sons, Inc.: New York, 2002, pp. 117–186.
[3] Matyjaszewski K, Tsarevsky NV. *Nat. Chem.* 2009, 1, 276–288.
[4] Osada Y, Bell AT, Shen M. *J. Polym. Sci. Pol. Lett.* 1978, 16, 309–311.
[5] Li B, Sun Q, Li G, Hou X. *Plasma Sci. Tech.* 1999, 1, 67.
[6] Liu YJ, Jiang XZ, Wang L. *Plasma Chem. Plasma P.* 2007, 27, 496–503.
[7] Elvira KS, i Solvas XC, Wootton RCR, deMello AJ. *Nat. Chem.* 2013, 5, 905–915.
[8] Yamanishi Y, Sameshima S, Kuriki H, Sakuma S, Arai F. In *2013 Transducers & Eurosensors XXVII: 17th International Conference on Solid-State Sensors, Actuators and Microsystems*, Barcelona, 2013, pp. 1795–1798.
[9] Bartolo D, Degré G, Nghe P, Studer V. *Lab. Chip* 2008, 8, 274–279.
[10] Priest C. *Biomicrofluidics* 2010, 4, 032206.
[11] Siegel AC, Shevkoplyas SS, Weibel DB, Bruzewicz DA, Martinez AW, Whitesides GM. *Angew. Chem.* 2006, 118, 7031–7036.
[12] Garstecki P, Fuerstman MJ, Stone HA, Whitesides GM. *Lab. Chip* 2006, 6, 437–446.
[13] Wu H, Sun P, Feng H, Zhou H, Wang R, Liang Y, Lu J, Zhu W, Zhang J, Fang J. *Plasma Process Polym.* 2012, 9, 417–424.
[14] Herron JT, Green DS. *Plasma Chem. Plasma P.* 2015, 21, 459–481.
[15] Baulch DL, Cobos CJ, Cox RA, Esser C, Frank P, Just T, Kerr JA, Pilling MJ, Troe J, Walker RW, Warnatz J. *J. Phys. Chem. Ref. Data* 1992, 21, 411–734.
[16] Finkelstein E, Rosen GM, Rauckman EJ. *J. Am. Chem. Soc.* 1980, 102, 4994–4999.
[17] Hibert C, Gaurand I, Motret O, Pouvesle JM. *J. Appl. Phys.* 1999, 85, 7070–7075.
[18] Bruggeman P, Schram DC. *Plasma Sources Sci. T.* 2010, 19, 045025.

[19] Djakaou IS, Ghezzar RM, Zekri MEM, Abdelmalek F, Cavadias S, Ognier S. *Plasma Chem. Plasma P.* 2014, 35, 143–157.
[20] Tatoulian M, Ognier S, Zhang M. European Patent, 2015, EP15306987.

Bionotes

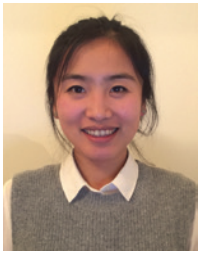

Mengxue Zhang

Mengxue Zhang is a PhD candidate at 2PM-IRCP, Chimie ParisTech (Paris, France), under the supervision of Prof. Michaël Tatoulian and Prof. Christophe Thomas. Her research mainly focuses on the interactions between plasma technologies and microfluidics applications. She received her BSc in 2011 and her MSc in 2013 at the Department of Chemical Engineering, Tsinghua University. She also holds a double degree of Ingénieur Généraliste from Ecole Centrale Marseille.

Stephanie Ognier

Stephanie Ognier is an associate professor of Université Pierre et Marie Curie (UPMC). She engages in the area of chemical engineering, with major works on cold-plasma-assisted processes (advanced oxidation processes and chemical synthesis). She defended her PhD at Montpellier 2 University in 2002.

Nadia Touati

Nadia Touati is a CNRS engineer. She is the technical manager of LASIR EPR platform at University Nord de France, Lille 1, since 2007. She has been working jointly with the PCMTH group at IRCP/CNRS in the structure of IR RPE RENARD network (CNRS) since 2014.

Laurent Binet

Laurent Binet is an associate professor at Chimie ParisTech (Paris, France). He is head of the Electron Paramagnetic Resonance (EPR) facility at LCMCP affiliated to the TGE-Renard French network. His major research field involves EPR of materials. He defended his PhD at Université Pierre et Marie Curie (UPMC) in 1995.

Christophe Thomas

Christophe Thomas is a professor at Chimie ParisTech (Paris, France). His research interests comprise the study of fundamental processes in organometallic chemistry with an emphasis on polymerization catalysis and the control of stereochemistry. He obtained his PhD degree in 2002 working under the supervision of Professor Süss-Fink (Switzerland). After postdoctoral experiences in Professor Coates' group at Cornell University (USA) and in Professor Ward's laboratories, he was appointed as Assistant Professor at the University of Rennes (France) in 2004. In 2008, he moved to Chimie ParisTech where he became a full professor in polymer chemistry. He is a junior member of the Institut Universitaire de France since 2012.

Patrick Tabeling

Patrick Tabeling is a research director of CNRS, professor at ESPCI (Paris, France), and director of the Institut Pierre-Gilles de Gennes pour la microfluidique (Paris, France). Since 2001, he is leader of the group MMN (Microfluidics MEMS and Nanostructures) composed of 20 researchers (permanents, PhDs, and Postdoctoral students). He has authored 200 papers, 11 patents (4500 citations, h factor 39), and 75 invited talks in international conferences. Since 2011, he is the director of the Institut Pierre-Gilles de Gennes, a new research institution dedicated to microfluidics and its applications.

Michaël Tatoulian

Michaël Tatoulian is a professor at Chimie ParisTech and leader of the research group 2PM (Processes, Plasmas, and Microsystems) at IRCP/CNRS. He is the author of 105 scientific papers, two patents, one keynote, two plenary presentations, and 24 invited talks. His major research areas concern the surface modification of different materials by plasma technology and the development of catalytic plasma microreactors and microfluidics.